Acta Materialia 128 (2017) 304–312

Contents lists available at ScienceDirect

Acta Materialia

journal homepage: www.elsevier.com/locate/actamat

Full length article

Temperature-dependent structure evolution in liquid gallium

L.H. Xiong [a], X.D. Wang [a, **], Q. Yu [a], H. Zhang [a, b], F. Zhang [c], Y. Sun [c], Q.P. Cao [a], H.L. Xie [d], T.Q. Xiao [d], D.X. Zhang [e], C.Z. Wang [c], K.M. Ho [c], Y. Ren [f], J.Z. Jiang [a, *]

[a] International Center for New-Structured Materials (ICNSM), Laboratory of New-Structured Materials, State Key Laboratory of Silicon Materials, and School of Materials Science and Engineering, Zhejiang University, Hangzhou, 310027, People's Republic of China
[b] Department of Chemical and Materials Engineering, University of Alberta, Edmonton, Alberta T6G 2V4, Canada
[c] Ames Laboratory, U.S. Department of Energy and Department of Physics and Astronomy, Iowa State University, Ames, IA 50011, USA
[d] Shanghai Institute of Applied Physics, Chinese Academy of Sciences, Shanghai, 201203, People's Republic of China
[e] State Key Laboratory of Modern Optical Instrumentation, Zhejiang University, Hangzhou, 310027, People's Republic of China
[f] Advanced Photon Source, Argonne National Laboratory, Argonne, IL 60439, USA

ARTICLE INFO

Article history:
Received 25 October 2016
Received in revised form
8 January 2017
Accepted 13 February 2017
Available online 17 February 2017

Keywords:
Structural evolution
Liquid gallium
Thermodynamical properties
X-ray diffraction
ab initio molecular dynamics

ABSTRACT

Temperature-dependent atomistic structure evolution of liquid gallium (Ga) has been investigated by using *in situ* high energy X-ray diffraction experiment and *ab initio* molecular dynamics simulation. Both experimental and theoretical results reveal the existence of a liquid structural change around 1000 K in liquid Ga. Below and above this temperature the liquid exhibits differences in activation energy for self-diffusion, temperature-dependent heat capacity, coordination numbers, density, viscosity, electric resistivity and thermoelectric power, which are reflected from structural changes of the bond-orientational order parameter Q_6, fraction of covalent dimers, averaged string length and local atomic packing. This finding will trigger more studies on the liquid-to-liquid crossover in metallic melts.

1. Introduction

Evolution of the temperature-dependent liquid structure is one of the long-standing issues [1–50]. With many efforts, the liquid-to-liquid crossover has been observed in several liquids, such as H_2O, C, P and Si [1–3,9,16,39,42,44,48,49]. Recently, it was also revealed in pure liquid Ce [20], supercooled liquid $Zr_{41.2}Ti_{13.8}Cu_{12.5}Ni_{10}Be_{22.5}$ [23] and liquid $La_{50}Al_{35}Ni_{15}$ [47], remaining as an intriguing but still elusive phenomenon in metallic liquids. For several monoatomic metallic liquids (i.e., Al, Zn, Sn and In), Lou et al. [21] found that the interatomic distances between the center atom and those on the first shell contract with increasing temperature, which promotes deeper understanding on the atomic structure evolution in metallic liquids [22,24–27,29,31–34,36–38,51]. The wide liquid region of gallium (Ga) with a low melting temperature (303 K) and extremely high boiling point (2477 K) at atmospheric pressure could facilitate a detailed study of its temperature-dependent liquid structure. Upon melting, the density of liquid Ga was higher than that of the stable crystalline phase [52]. X-ray and neutron scattering analyses indicated that the first peak in structure factor $S(q)$ is indeed asymmetric with a shoulder at its high-momentum side, which is quite distinguishing from other metallic melts [53,54]. By X-ray diffraction (XRD) measurements, the first peak sharpened in the supercooled liquid Ga as cooling the temperature from 323 to 273 K, while the main peak moved to the left side and the shoulder became less discernible with increasing temperature in the range of 283–973 K [55,56]. For liquid Ga, the balance between metallic and covalent tendencies could be altered via temperature, pressure and impurities. The coexistence of monatomic and diatomic molecular fluid characteristics in liquid Ga was found to be similar to that in the α-Ga rather than the β-Ga revealed by *ab initio* molecular dynamics simulations [57]. The covalently-bonded Ga-Ga dimers could persist into high temperature. The presence of the shoulder on the right side of the main peak suggested that the ordering caused by Friedel oscillations within a nanoscale range could still persist in the liquid state [58]. Up to now, however, the possible

* Corresponding author.
** Corresponding author.
E-mail addresses: wangxd@zju.edu.cn (X.D. Wang), jiangjz@zju.edu.cn (J.Z. Jiang).

http://dx.doi.org/10.1016/j.actamat.2017.02.038
1359-6454/

liquid structural change in the higher temperature of liquid Ga has not been systematically studied in a wide temperature region, and it remains the long-standing ambiguity.

Here we report the results of an intriguing temperature-induced liquid structural change in liquid Ga detected by *in-situ* high energy XRD experiments and *ab initio* molecular dynamics (AIMD) simulations. XRD measurements were carried out in the transmission mode at the 11-1D-C beamline of Advanced Photon Source (APS) when the sample was studied at the temperature range of 400–1373 K. Meanwhile, AIMD simulations were performed to reproduce the three-dimensional atomic configurations. Structural examinations reveal that two liquid regimes below and above the critical temperature of about 1000 K having distinct differences in diffusion activation energies and heat capacities, show changes in coordination number, bond-orientational order, fractions of covalent dimers, string length and atomic packing. Previous reported data of density [59], viscosity [60], electric resistivity and absolute thermoelectric power [61,62] of liquid Ga also support our observation, which could further deepen the understanding of liquids.

2. Experimental and computational details

High-purity Ga (99.999%) rod was filled into thin-wall (thickness of 0.01 mm) capillaries with 1.5 mm in diameter. The capillaries with samples inside were then vacuumed to 8.6×10^{-4} Pa and immediately sealed. The sealed capillaries were placed at the center of heating furnace. When the sample was continuously heating with a rate of 10 K/min, the diffraction patterns were recorded by a flat-panel Si detector (Perkin-Elmer 1621) with 200×200 μm^2 pixel size and 2048×2048 pixels at the 11-ID-C of Advanced Photon Source (APS) with a wavelength of 0.117 Å and the beam size of 0.3×0.3 mm^2. The incident beam flux was recorded for the normalization. The acquisition time was 1s for each diffraction pattern and every 20 patterns were summed to output one diffraction file. The sample remained metallic shining after measurements, and its XRD pattern is also similar to that of the starting sample. The uncertainty of the temperature for one XRD pattern is about ±3 K. Scattering intensities $I(q)$ were integrated under the software package FIT2D, and the experimental structure factors $S(q)$ were derived from $I(q)$ by subtracting the appropriate background and correcting for oblique incidence, absorption, sample geometry, multiple scattering, fluorescence, Compton scattering and secondary container-scattering contributions by using the program PDFgetX2 [63,64]. The experimental densities of liquid Ga were adopted for the pair-distribution functions and coordination number calculations [65]. Similar process could be found elsewhere [66–68].

Ab initio molecular dynamic simulations of liquid Ga were undertaken by using the Vienna *ab initio* simulation package (VASP) [69,70]. The simulations were performed with the canonical NVT ensemble (constant number, volume and temperature); and the temperature was controlled by the Nosé-Hoover thermostat [71,72]. Only the Γ point was considered to sample the Brillouin zone in the simulations since the simulation box was sufficiently large. The interaction between electrons and ions was modelled by a Projector Augmented-Wave (PAW) method [73]. The general gradient approximation (GGA) in the form by Pedrew-Burke-Ernzerhof (PBE) was used for the exchange-correlation energy functional [74]. An energy cutoff of 134.68 eV was used for the plane-wave basis set to expand the wave function, and a typical time interval of 3 fs was applied with the Verlet algorithm to integrate Newton's equations of motion. A cubic box with periodic boundary condition, containing 216 Ga atoms, was fully melted at 2000 K (well above its melting point) to remove the crystalline symmetry and reach thermal equilibrium, followed by step-wise cooling to 1900, 1800, 1700, 1600, 1500, 1400, 1300, 1200, 1100, 1000, 900, 800, 700, 600, 500 and 400 K successively with a rate of 0.1 K per MD step. At each temperature, the system was thermally equilibrated, and the internal pressure was maintained almost zero by adjusting the box size. Afterwards, an additional 12000 MD steps were performed for statistical analyses at each temperature.

3. Results and discussion

3.1. Structural factor and pair-distribution function

It is of significant importance to unveil the local structure evolution or transition of metallic liquids as heated above several times of the melting point. Applying high-temperature and high-energy synchrotron XRD measurements, one can get high-resolution quality data sets to analyze and extract the structural information. On the basis of structure factor, we investigate the peak position evolution of first sharp diffraction peak of liquid Ga obtained from synchrotron XRD experiments, as shown in Fig. 1. A shoulder is visible on the first peak at low temperatures and still well-pronounced at higher temperatures [53,54]. Considering the asymmetry of the first peak in $S(q)$, two individual peak profiles are applied to fit the first main peak and its shoulder, which was also reported in literature [75–78]. Fitting results at two selected temperatures are presented in Fig. 2, in which experimental data can be well fitted so that more detailed information could be extracted. Fig. 1(b) shows the positions of the first main peak and its shoulder in $S(q)$ curves obtained by XRD measurements as a function of temperature, which clearly show a non-linear evolution with

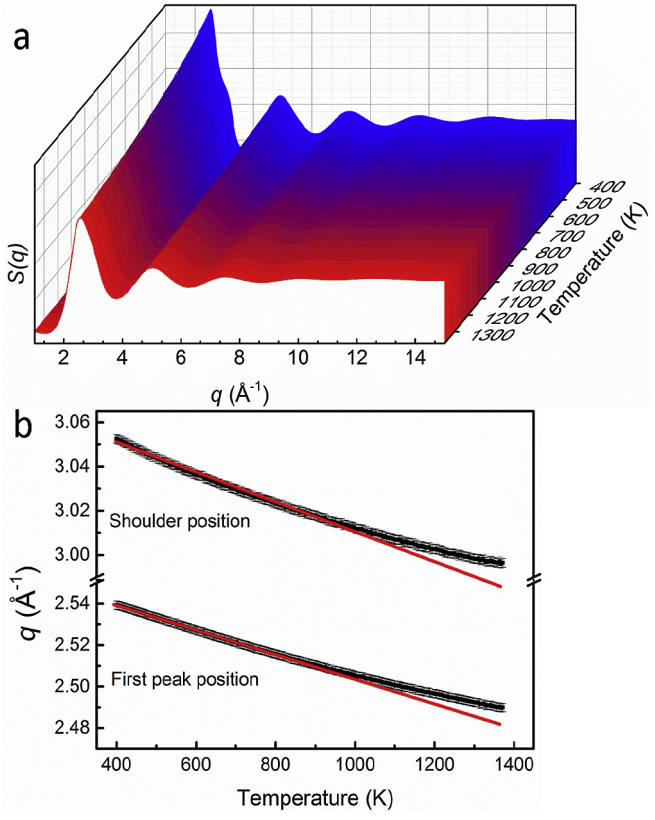

Fig. 1. **a** Waterfall graphs of structure factors of liquid Ga obtained from *in-situ* high-temperature XRD at different temperatures. **b** The peak positions of the main and shoulder components for the first peak as a function of temperature. As guided by the lines, a deviation from the linear relationship obviously appears both at the positions of main peak and its shoulder vs. temperature. The error bars are estimated from the standard deviation of the fitting.

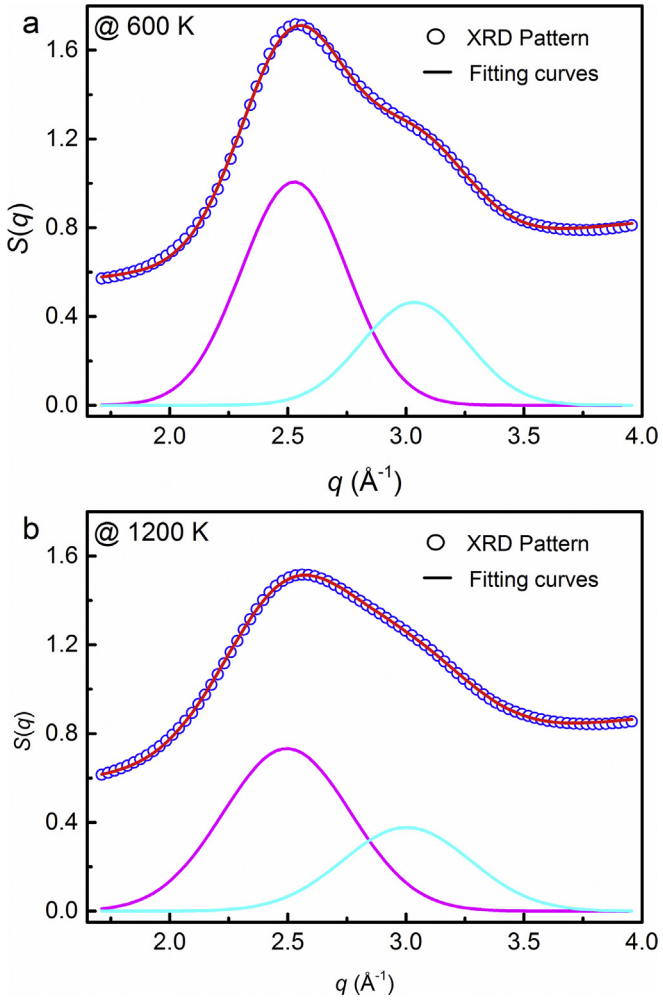

Fig. 2. Fitting (red curve) of the first structure factor maximum (blue open circle) using two Gaussian functions (magenta and cyan curves) at 600 and 1200 K. The baseline is corrected prior to fitting. (For interpretation of the references to colour in this figure legend, the reader is referred to the web version of this article.)

temperature in the whole studied temperature range. During heating from 400 to 1373 K, the positions of the first main peak and its shoulder decrease gradually. By a carefully examination, it is found that data below about 1000 K can be fitted by a linear line while a deviation of data from the linear line is detected at temperatures above about 1000 K. As an important physical quantity to describe the structure of liquids, pair-distribution functions $G(r)$ of liquid Ga on the dependence of temperature is shown in Fig. 3. Similarly, a deviation of the first main peak position and its shoulder position (Fig. 3(b)) and the coordination number (CN, Fig. 3(c)) from the linear lines below about 1000 K is detected at temperatures above about 1000 K. Heating from 400 K, the interatomic distance of the first main peak and CN decrease corresponding to a contraction in the first coordination shell instead of expansion, similar results reported for other metallic liquids [21], while the interatomic distance of the shoulder position increases. However, when the temperature increases above about 1000 K, the centers of these two peaks and CN continue to shift but at different rates, indicating a change in the local atomic structure in liquid Ga below and above about 1000 K.

3.2. Local atomistic structure

In order to elucidate the structure change at an atomistic scale,

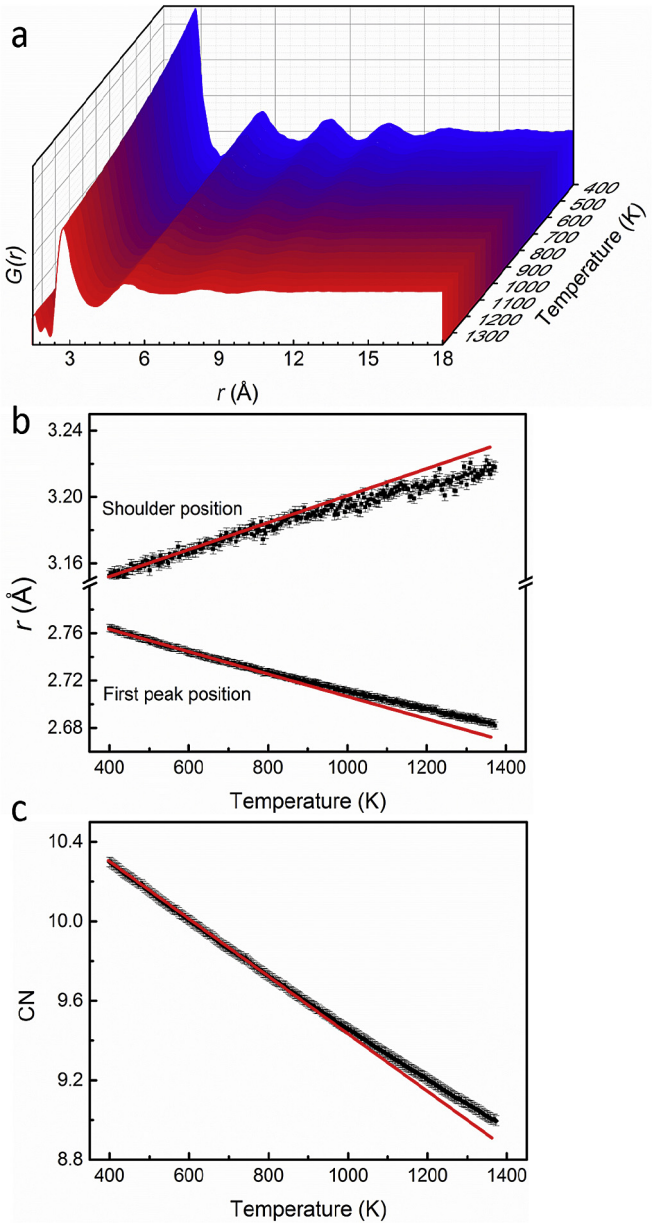

Fig. 3. **a** Waterfall graphs of pair-distribution functions of liquid Ga obtained from *in-situ* high-temperature XRD at various temperatures. **b** The peak positions of the main and shoulder components for the first peak as a function of temperature. **c** The evolution of coordination number on the dependence of temperature. Guided by the lines, a deviation from the linear relationship obviously exhibits among at the positions of main peak and its shoulder and coordination number vs. temperature. The error bars are estimated from the standard deviation of the fitting.

we performed AIMD simulations to reproduce the three-dimensional configurations at various temperatures, as demonstrated in Fig. 4 at four selected temperatures. Although slight differences between theoretical and experimental data were observed, the structural factor and pair-correlation functions data obtained from AIMD simulations and XRD measurements match very well with each other in terms of peak positions, amplitudes and shapes, which validate structural analyses in the following parts. To describe local bond-orientational order (BOO), the spherical harmonics analysis was firstly introduced by Steinhardt et al., and the coarse-grained form was adapted by Lechner [13,79]. The $(2l + 1)$ dimensional complex vector (q_l) can be defined for

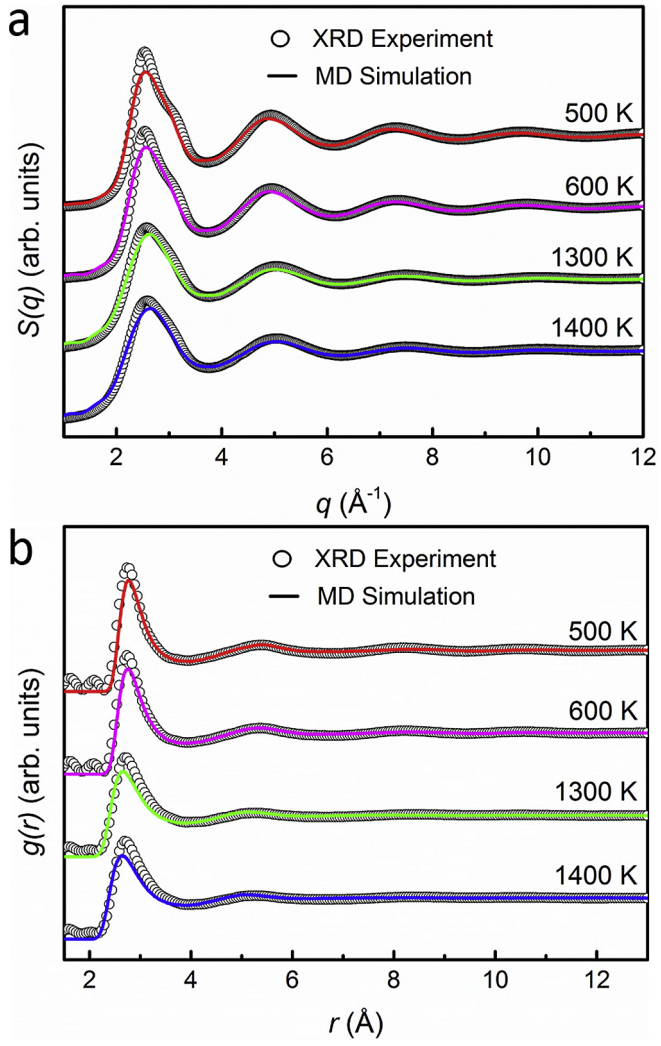

Fig. 4. At four selected temperatures, the comparison of structure factors and pair-correlation functions between experiments and simulations gives an excellent match, which strongly validate atomistic structure analyses.

each atom i as presented in Eq. (1).

$$q_{lm}(i) = \frac{1}{N_b(i)} \sum_{j=1}^{N_b(i)} Y_{lm}\left(\hat{r}_{ij}\right) \tag{1}$$

where l is the free integer parameter, m is an integer that runs from -l to l, Y_{lm} are the spherical harmonics, $\hat{r}_{ij}$ is the vector from atom i to atom j, and the sum goes over all neighboring atoms $N_b(i)$ of atom i. We could average the spatially local bond order parameters according to the equation $\hat{q}_{lm}(i) = \frac{1}{N_b(i)} \sum_{j=1}^{N_b(i)} q_{lm}(k)$, and construct the rotationally invariant quantities, as demonstrated in Eq. (2).

$$Q_l(i) = \sqrt{4\pi/(2l+1)} \left| \hat{q}_{lm}(i) \right| \tag{2}$$

It should be noted that Mickel pointed out the two flaws of Steinhardt order parameters: one is the definition of the nearest neighboring spheres around a given central particle, the other is the discontinuous function of the particle coordinates [80]. After the modification by Lechner, such two shortcomings are avoided by averaging the first neighbor shell of a given particle and the particle itself. The averaged parameters (BOO) are very sensitive to measure the different bond-orientational symmetries and differentiate the local atomic environment. Fig. 5(a) illustrates the BOO parameter Q_6 at various temperatures, showing a local minimum at about 1000 K when the temperature cools down from 2000 K to 400 K. In general, the bond-orientational order reflects the relative orientation of the geometrical bonds between a particle and its neighboring particles [19]. The Q_6 values are usually larger in highly

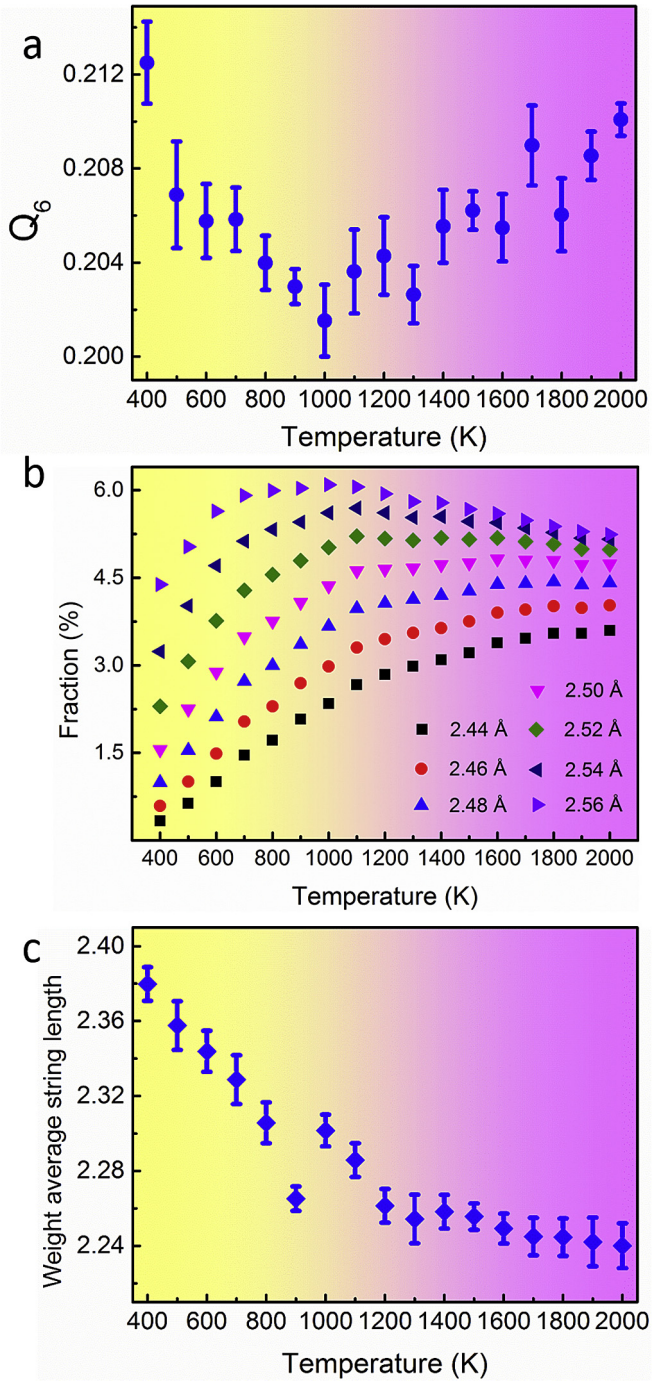

Fig. 5. (a) The bond orientation order parameter Q_6 versus temperature in liquid Ga. (b) The fractions of covalently-bonded dimers with temperature using different cutoff values from 2.44 to 2.56 Å in liquid Ga. (c) The weight-averaged string length as a function of temperature from 400 to 2000 K in liquid Ga. The error bars are taken from the standard deviation in the statistical analysis of AIMD configurations. The shadow zone demonstrates the emergence of the structural change.

crystalline-like regions, and become lower in disordered liquids. However, the Q_6 value for liquid Ga exhibits a minimum at about 1000 K, indicating that the local geometry orientations in liquid Ga experiences a crossover during cooling from high temperature region to low temperature region. Such two liquid regions in liquid Ga should have differences of other properties.

Liquid Ga behaves both covalent and metallic characteristics. The covalently-bonded dimers are the atomic pairs whose coordination number is one within the cutoff distance. We statistically analyze the interatomic surroundings of a given atom in liquid Ga and the atoms with only one neighbor atom within the cutoff distance are counted. Note that in the literature the interatomic distance of the covalently-bonded dimers is reported to be 2.484 Å in Ga [57,58]. By considering the temperature dependent interatomic distance of dimers, different cutoff values from 2.44 to 2.56 Å were applied to track the fraction evolution of dimers in the liquid Ga in Fig. 5(b). Upon heating from 400 K, no matter of the cutoff value selected, the fraction of dimers increases largely, it then converts to a flat plateau when the temperature arises above about 1000 K. Thus, distinct differences in the temperature dependent fraction of dimers are detected in both low and high temperature regions in liquid Ga, separated at about 1000 K, which is consistent with the observed minimum of BOO parameter Q_6 (Fig. 5(a)), deviations from linear relationship in structure factor (Fig. 1(b)), pair-distribution functions (Fig. 3(b)) and coordination numbers (Fig. 3(c)). We believe that structural differences in both temperature regions should also affect the dynamics of liquid Ga, which will be discussed in the following section.

The cooperative dynamics analysis based on the atomic motion, is to quantify the collective atomic displacement motion [81]. Firstly, we define the mobile atoms by comparing the self-part of the van Hove correlation function to an ideal uncorrelated liquid, of which the moving distance $r(t)$ is larger than the particular amplitude of an atomic vibration after a decorrelation time t^*, but smaller than a typical distance, i.e., a $< r_i(\Delta t) - r_i(0) < b$, where $r_i(t)$ denotes the atomic position of atom i at time t. If $\min[|r_i(\Delta t) - r_j(0)|, |r_i(0) - r_j(\Delta t)|] < \delta$, where δ is the half distance of the average atomic distance, mobile atoms i and j are spatially considered to be collective relations. Since the cooperative particle dynamic is one characteristic feature of the dynamics in liquids, the weight average string length as a function of temperature is shown in Fig. 5(c). The average string length decreases as the temperature increases. However, a distinct kink occurs at about 1000 K, changing the dropping slope to a small value.

The recently-developed cluster alignment method describes the local atomic packing and provides more insights into the average structure in the liquid and disordered systems [82]. This method has been applied to directly visualize the average local short-range order and medium range order [83–85]. Thus, the cluster alignment method is applied to further elucidate the short-range order difference between high- and low-temperature regions in liquid Ga. 2000 clusters are randomly selected from the AIMD simulation trajectories at four selected temperatures of 600, 1000, 1200 and 1600 K. Each cluster consists of 16 atoms. These clusters are then rigidly rotated and aligned to each other until the overall mean-square distances is minimized. Finally, the distributions of the atoms after the collective alignment are smoothed by a Gaussian smearing scheme to obtain three-dimensional atomic density distributions, which is the three-dimensional representation of average short-range order. Fig. 6 depicts the local structures of liquid Ga at the selected four temperatures. At 1600 K, the aligned clusters exhibit weak short-range order, indicating a highly disordered structure. The local short-range order enhances upon cooling and rapidly dominates at temperature below about 1000 K. At 600 K, the crystalline orthorhombic-like local atomic packing is detected in liquid Ga. This clearly unveils that the local atomic packing at low temperature region (below about 1000 K) in liquid Ga breaks up during heating and displays more disordered atomic packing structure at high temperature region (above about 1000 K), in consistent with the above-mentioned results.

3.3. Thermodynamical properties

Using the Stokes-Einstein relation, the diffusion coefficient of liquid Ga was estimated from the mean square displacement function in AIMD simulations. The self-diffusion coefficient D of gallium was subtracted from AIMD simulations for the long time (36 ps) annealing at each temperature. A linear mean square displacements as the function of time could be found in this study, which is defined by $< r^2(t) > = < \left| r_i(t) - r_i(0) \right|^2 >$, where $r_i(t)$ is the atomic position of atom i at time t. The self-diffusion coefficient D can be calculated by Eq. (3).

$$D = \lim_{t \to \infty} \frac{< r^2(t) >}{6t} \tag{3}$$

Fig. 7(a) illustrates diffusion coefficients of liquid Ga at various temperatures. According to the Arrhenius equation, two activation energies are found to be about 15.78 kJ/mol in the range of 1100–2000 K and 8.12 kJ/mol in 400–1000 K. The activation energy in the low temperature range is much less than that in the high temperature range in sharp contrast to the common sense that the activation energy for a uniform liquid should be lower at high temperatures. This also indicates the existence of a structural change in liquid Ga at around 1000 K. In the inset of Fig. 7(a), a kink at around 1000 K is also detected based on the total energy change for the liquid Ga obtained from AIMD.

As one of the most basic quantities to be taken into consideration as the dependence of temperature in phase transitions, the heat capacity C_v in AIMD simulations for the canonical ensemble could be calculated by Eq. (4) [82].

$$C_V(T) = \frac{1}{k_B T^2} \left(\left\langle E^2 \right\rangle - \langle E \rangle^2 \right) \tag{4}$$

where $\langle E \rangle$ is the average ensemble of free energy E. Fig. 7(b) shows the temperature-dependent heat capacity C_v of liquid Ga. It is found that the heat capacity increases very slowly (almost unchanged) from 2000 K to 1100 K, but distinctly rises below about 1000 K. The similar trend is usually observed for the supercooled liquids before the glass transition rather than the overheated liquids [16,50], further implying the existence of the local structure change at around 1000 K in liquid Ga. It should be pointed out that the studied temperature range of 400–2000 K is higher than the melting point of pure Ga. The inset in Fig. 7(b) shows the CN of the nearest neighbors estimated from AIMD results as a function of temperature. The CN value generally decreases as the temperature increases, similar to the experimental data in Fig. 2(c), in which a kink in the temperature dependent CN is also detected at about 1000 K.

In addition, Fig. 8(a) shows the density data of liquid Ga measured by gamma-ray absorption method [59], guided by the dashed lines. In fact, a kink also exists at about 1000 K. As shown in Fig. 8(b), such a break of agreement between the experimental viscosity points of liquid Ga and Enskog's theory at around 1000 K is also found in the viscosity measurement by Tippelskirch using oscillating cup method [60]. Electrical resistivity of liquid Ga in Fig. 8(c) and absolute thermoelectric power of liquid Ga in Fig. 8(d), which are sensitive to structural change in liquids, also suggest

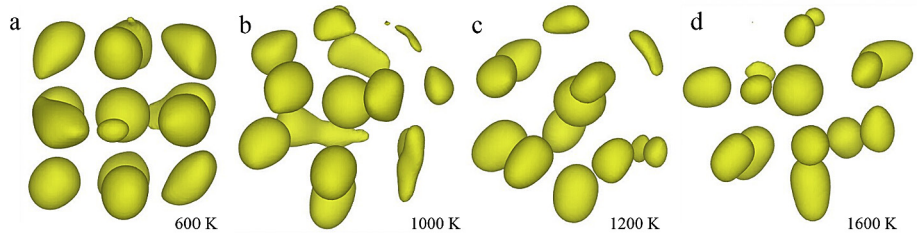

Fig. 6. Atomistic morphology evolution in liquid Ga obtained from the cluster alignment method at selected four temperatures of 600, 1000, 1200 and 1600 K at the iso-surface value of 0.021.

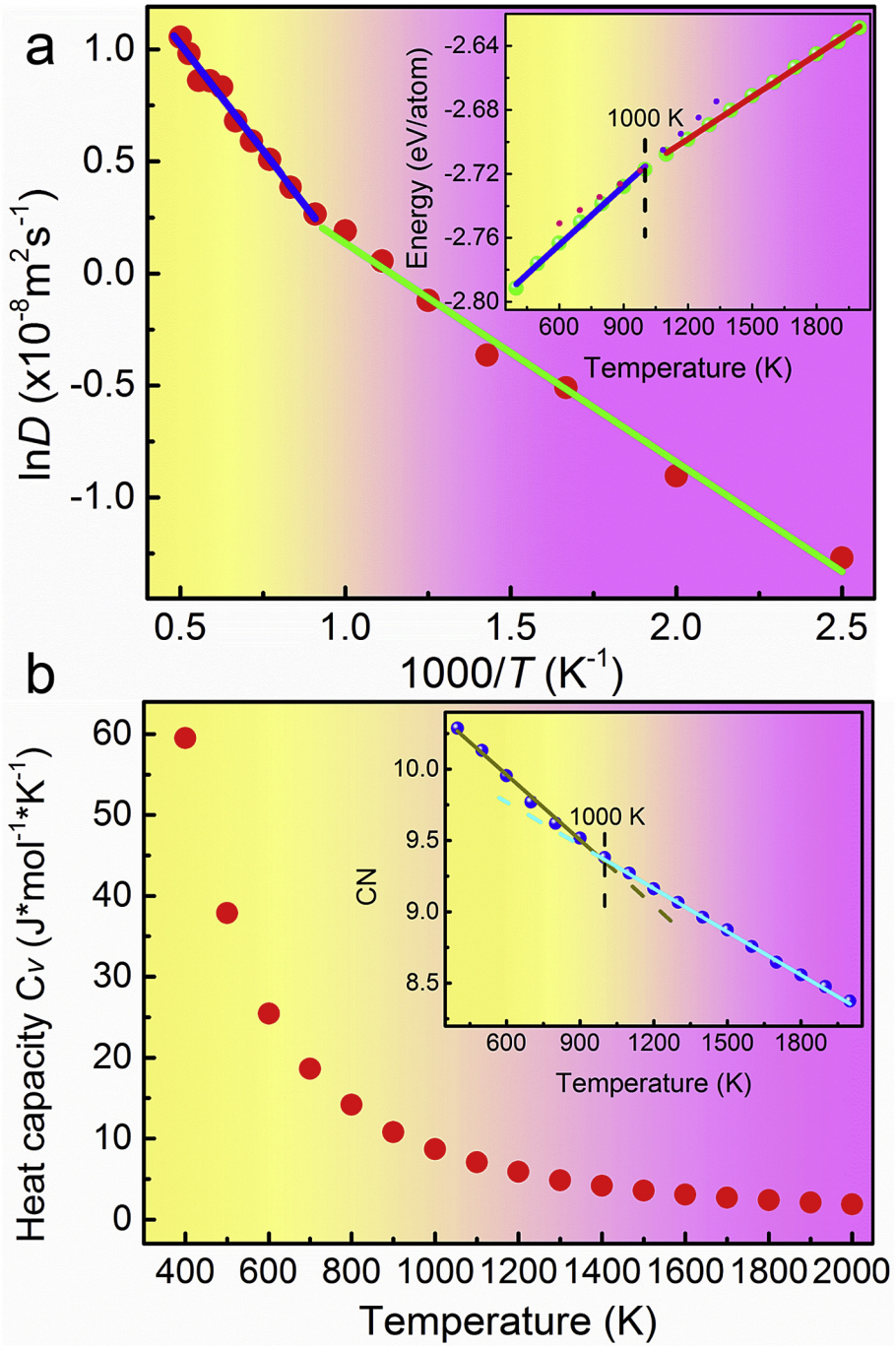

Fig. 7. (a) Diffusion coefficient of liquid Ga from 2000 to 400 K obtained from AIMD simulations. The shadow regime illustrates a crossover of activation energy from 15.78 kJ/mol to 8.12 kJ/mol. (b) Heat capacity C_v of liquid Ga calculated by AIMD simulations. The shadow region separates two parts: one plateau in higher-temperature range, the other sharp increasing below the critical temperature. The inset shows the discontinuous evolution of coordination number guided by the lines to display a change at 1000 K.

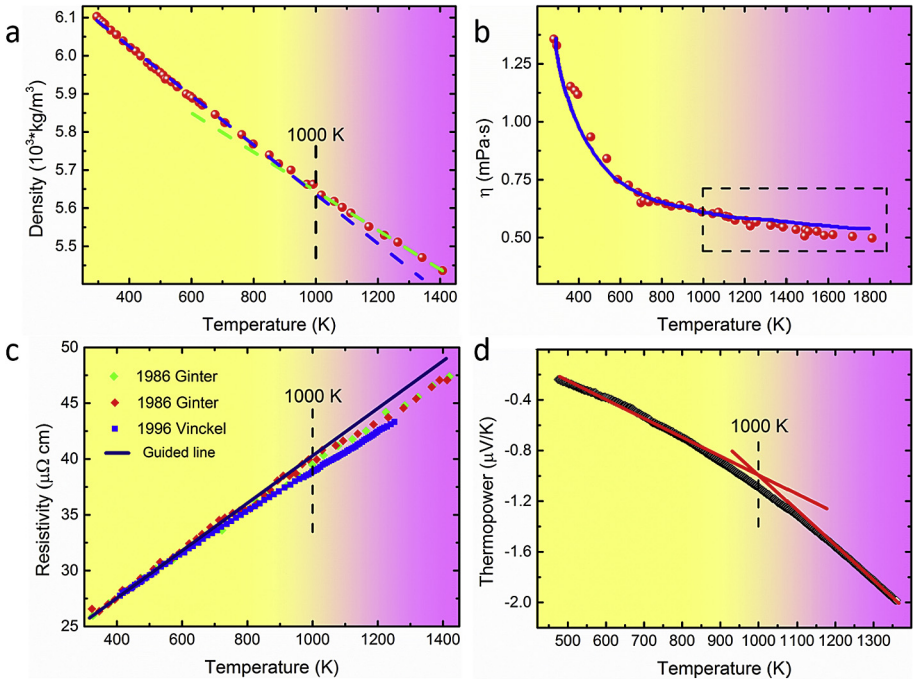

Fig. 8. Thermophysical properties of liquid Ga. **a** Density of liquid Ga by the gamma absorption method on the dependence of temperature [59]. As guided by the dashed lines, a discontinuous change appears at about 1000 K **b** Viscosity of liquid Ga as the dependence of temperature measured by the oscillating cup method [60]. A break of agreement between the experimental points and Enskog's theory could be found above 1000 K marked by the dash lines. **c** Electrical resistivity of liquid Ga reported in different references on the dependence of temperature [61,62]. As guided by the line, a deviation from linear relationship appears at about 1000 K. **d** Absolute thermoelectric power of liquid Ga as the function of temperature [62]. A change of two different parts could be found around 1000 K marked by the red guided lines. (For interpretation of the references to colour in this figure legend, the reader is referred to the web version of this article.)

different temperature dependences of such properties below and above around 1000 K [61,62]. The electric resistivity starts to deviate from the linear relationship at about 1000 K. The absolute thermoelectric power splits into two parts at around 1000 K as increasing the temperature. Different temperature dependences of density, viscosity, electric resistivity, thermoelectric power, diffusion activation energy, heat capacity, coordination number, the first peak position of structure factor and pair-distribution functions are observed at low- and high-temperation regions in liquid Ga, separated at around 1000 K. All these properties and structural results obtained from both experiments here and literature, and theoretical calculations here uncover a liquid-to-liquid crossover separated at around 1000 K in liquid Ga.

In spite of the long-standing open issue of the liquid-liquid phase transition, increasing attentions have been attracted upon the research of liquid structural evolution. Tanaka held the view that liquid is not homogeneous and in liquids locally favored structures exist [86]. The nearest-neighbor coordination difference leaves space of local structural variation of chemical and topological order. Thus, the short-range order (even medium-range order) of liquid might vary with temperatures, causing the change of thermodynamical properties (like the diffusion activation energy and heat capacity of liquid Ga). When cooled below the melting temperature, a remarkable slowdown of the thermal dynamics in the supercooled liquid mostly can be observed. Structural evolutions of metallic glass-forming liquids during vitrification are consistent with the transformation from stable liquid to metastable liquid [78,87]. During cooling below the equilibrium liquidus temperature, metallic liquids usually exhibit a rapid rise in viscosity and non-Arrhenius temperature dependence of viscosity characterized by the fragility of liquid, correlated to the anomalies in the evolution of the atomic structure in the supercooled liquid region [75,76]. The populations of atomic clusters with icosahedral local symmetry become predominant as glass transition temperature is approached and facilitate vitrification and suppression of crystal nucleation and growth, correlated to the fragile to strong transition. Correlations of structural parameters (such as structure factor and viscosity) with the notion of fragile-strong transition as the dependence of temperature were reported [77,88]. However, it might be a different behavior when the temperature is higher than melting temperature [23]. This work focuses on the pure liquid of Ga above its melting temperature. It could be true that the behavior of liquid Ga in the temperature range above melting temperature differs from that for undercooled liquid Ga. These results clearly motivate the need for further investigation in the undercooled Ga liquid.

4. Conclusions

In summary, the evolution of atomic structure in the liquid Ga has been studied by high-temperature and high-energy XRD measurements and AIMD simulations. An intriguing liquid structural change between two different Ga liquid regimes is discovered at the critical temperature of about 1000 K. Below this temperature, the liquid Ga has an activation energy of 8.12 kJ/mol for self-diffusion coefficient, a large increasing slope of peak position shift of the first peak in structure factor and pair-distribution functions, a distinct increase of BOO parameter Q_6, heat capacity, and weight averaged string length with decreasing temperature, resulting from the high-coordinated orthorhombic-like atomic packing. Above this temperature, the liquid exhibits an activation energy of 15.78 kJ/mol for self-diffusion coefficient, a small reducing slope of peak-position shift of the first peak in structural factor and pair-distribution functions, an increase of BOO parameter Q_6 with elevating temperature, and flat temperature-dependent heat capacity and insensitive weight average string

length for forming the low-coordinated disordered polyhedrons. This discovery in pure element Ga will further trigger more studies for the liquid-to-liquid crossover in metallic liquids.

Acknowledgements

The authors thank Dr. S. Sastry for valuable discussion. Financial supports from the National Natural Science Foundation of China (51371157, U1432105, U1432110, U1532115, 51671170 and 51671169), the National Key Research and Development Program of China (No. 2016YFB0701203 and 2016YFB0700201), the Natural Science Foundation of Zhejiang Province (grants Z1110196 and Y4110192), and the Fundamental Research Funds for the Central Universities are gratefully acknowledged. The computer resources at National Supercomputer Centers in Tianjin and Guangzhou are also gratefully acknowledged. The studies performed at the Ames Laboratory were supported by the US Department of Energy, Basic Energy Sciences, Division of Materials Science and Engineering, under Contract No. ED-AC02-07CH11358, including a grant of computer time at the National Energy Research Supercomputing Center (NERSC) in Berkeley, CA.

References

[1] O. Mishima, H.E. Stanley, The relationship between liquid, supercooled and glassy water, Nature 396 (1998) 329–335.
[2] J.N. Glosli, F.H. Ree, Liquid-liquid phase transformation in carbon, Phys. Rev. Lett. 82 (1999) 4659.
[3] Y. Katayama, T. Mizutani, W. Utsumi, O. Shimomura, M. Yamakata, K. Funakoshi, A first-order liquid-liquid phase transition in phosphorus, Nature 403 (2000) 170–173.
[4] H. Reichert, O. Klein, H. Dosch, M. Denk, V. Honkimäki, T. Lippmann, G. Reiter, Observation of five-fold local symmetry in liquid lead, Nature 408 (2000) 839–841.
[5] P.G. Debenedetti, F.H. Stillinger, Supercooled liquids and the glass transition, Nature 410 (2001) 259–267.
[6] N. Jakse, A. Pasturel, Local order of liquid and supercooled zirconium by ab initio molecular dynamics, Phys. Rev. Lett. 91 (2003) 195501.
[7] K.F. Kelton, G.W. Lee, A.K. Gangopadhyay, R.W. Hyers, T.J. Rathz, J.R. Rogers, M.B. Robinson, D.S. Robinson, First x-ray scattering studies on electrostatically levitated metallic liquids: demonstrated influence of local icosahedral order on the nucleation barrier, Phys. Rev. Lett. 90 (2003) 195504.
[8] J. Nord, K. Albe, P. Erhart, K. Nordlund, Modelling of compound semiconductors: analytical bond-order potential for gallium, nitrogen and gallium nitride, J. Phys. Condens. Matter 15 (2003) 5649.
[9] S. Sastry, C.A. Angell, Liquid-liquid phase transition in supercooled silicon, Nat. Mater. 2 (2003) 739–743.
[10] G.W. Lee, A.K. Gangopadhyay, K.F. Kelton, R.W. Hyers, T.J. Rathz, J.R. Rogers, D.S. Robinson, Difference in icosahedral short-range order in early and late transition metal liquids, Phys. Rev. Lett. 93 (2004) 037802.
[11] P.F. McMillan, M. Wilson, D. Daisenberger, D.A. Machon, A density-driven phase transition between semiconducting and metallic polyamorphs of silicon, Nat. Mater. 4 (2005) 680–684.
[12] T. Egami, Icosahedral order in liquids, J. Non Cryst. Solids 353 (2007) 3666–3670.
[13] W. Lechner, C. Dellago, Accurate determination of crystal structures based on averaged local bond order parameters, J. Chem. Phys. 129 (2008) 114707.
[14] X.J. Liu, Y. Xu, X. Hui, Z.P. Lu, F. Li, G.L. Chen, J. Lu, C.T. Liu, Metallic liquids and glasses: atomic order and global packing, Phys. Rev. Lett. 105 (2010) 155501.
[15] C. Zhang, L. Hu, Y. Yue, J.C. Mauro, Fragile-to-strong transition in metallic glass-forming liquids, J. Chem. Phys. 133 (2010) 014508.
[16] V.V. Vasisht, S. Saw, S. Sastry, Liquid-liquid critical point in supercooled silicon, Nat. Phys. 7 (2011) 549–553.
[17] Z. Evenson, T. Schmitt, M. Nicola, I. Gallino, R. Busch, High temperature melt viscosity and fragile to strong transition in Zr-Cu-Ni-Al-Nb(Ti) and $Cu_{47}Ti_{34}Zr_{11}Ni_8$ bulk metallic glasses, Acta Mater. 60 (2012) 4712–4719.
[18] K.N. Lad, N. Jakse, A. Pasturel, Signatures of fragile-to-strong transition in a binary metallic glass-forming liquid, J. Chem. Phys. 136 (2012) 104509.
[19] J. Russo, H. Tanaka, The microscopic pathway to crystallization in supercooled liquids, Sci. Rep. 2 (2012) 505.
[20] A. Cadien, Q.Y. Hu, Y. Meng, Y.Q. Cheng, M.W. Chen, J.F. Shu, H.K. Mao, H.W. Sheng, First-order liquid-liquid phase transition in cerium, Phys. Rev. Lett. 110 (2013) 125503.
[21] H.B. Lou, X.D. Wang, Q.P. Cao, D.X. Zhang, J. Zhang, T.D. Hu, H.K. Mao, J.Z. Jiang, Negative expansions of interatomic distances in metallic melts, Proc. Natl. Acad. Sci. 110 (2013) 10068–10072.
[22] M. Mayo, E. Yahel, Y. Greenberg, G. Makov, Short range order in liquid pnictides, J. Phys. Condens. Matter 25 (2013) 505102.
[23] S. Wei, F. Yang, J. Bednarcik, I. Kaban, O. Shuleshova, A. Meyer, R. Busch, Liquid-liquid transition in a strong bulk metallic glass-forming liquid, Nat. Commun. 4 (2013) 2083.
[24] T. Debela, X.D. Wang, Q.P. Cao, D.X. Zhang, S.Y. Wang, C.Z. Wang, J.Z. Jiang, Atomic structure evolution during solidification of liquid niobium from ab initio molecular dynamics simulations, J. Phys. Condens. Matter 26 (2014) 055004.
[25] J. Ding, M. Xu, P.F. Guan, S.W. Deng, Y.Q. Cheng, E. Ma, Temperature efforts on atomic pair distribution functions of melts, J. Chem. Phys. 140 (2014) 064501.
[26] M. Emuna, M. Mayo, Y. Greenberg, E.N. Caspi, B. Beuneu, E. Yahel, G. Makov, Liquid structure and temperature invariance of sound velocity in supercooled Bi melt, J. Chem. Phys. 140 (2014) 094502.
[27] Z. Evenson, S.E. Naleway, S. Wei, O. Gross, J.J. Kruzic, I. Gallino, W. Possart, M. Stommel, R. Bush, β relaxation and low-temperature aging in a Au-based bulk metallic glass: from elastic properties to atomic-scale structure, Phys. Rev. B 89 (2014) 174204.
[28] A.K. Gangopadhyay, M.E. Blodgett, M.L. Johnson, J. McKnight, V. Wessels, A.J. Vogt, N.A. Mauro, J.C. Bendert, R. Soklaski, L. Yang, K.F. Kelton, Anomalous thermal contraction of the first coordination shell in metallic alloy liquids, J. Chem. Phys. 140 (2014) 044505.
[29] A.K. Gangopadhyay, M.E. Blodett, M.L. Johnson, A.J. Vogt, N.A. Mauro, K.F. Kelton, Thermal expansion measurements by x-ray scattering and breakdown of Ehrenfest's relation in alloy liquids, Appl. Phys. Lett. 104 (2014) 191907.
[30] L.B. Skinner, C.J. Benmore, J.K.R. Weber, M.A. Williamson, A. Tamalonis, A. Hebden, T. Wiencek, O.L.G. Alderman, M. Guthrie, L. Leibowitz, J.B. Parise, Molten uranium dioxide structure and dynamics, Science 346 (2014) 984–987.
[31] J. Tan, G. Wang, Z.Y. Liu, J. Bednarcik, Y.L. Gao, Q.J. Zhai, N. Mattern, J. Eckert, Correlation between atomic structure evolution and strength in a bulk metallic glass at cryogenic temperature, Sci. Rep. 4 (2014) 3897.
[32] Y. Wang, Y.H. Lu, X.D. Wang, Q.P. Cao, D.X. Zhang, J.Z. Jiang, Effects of spin orbital coupling on atomic and electronic structures in Al_2Cu and Al_2Au crystal and liquid phases via ab initio molecular dynamics simulations, J. Alloy Compd. 613 (2014) 55–61.
[33] L.H. Xiong, H.B. Lou, X.D. Wang, T.T. Debela, Q.P. Cao, D.X. Zhang, S.Y. Wang, C.Z. Wang, J.Z. Jiang, Evolution of local atomic structure during solidification of Al_2Au liquid: an ab initio study, Acta Mater. 68 (2014) 1–8.
[34] W.M. Yang, J.W. Li, H.S. Liu, C.C. Dun, H.L. Zhang, J.T. Huo, L. Xue, Y.C. Zhao, B.L. Shen, L.M. Dou, A. Inoue, Origin of abnormal glass transition behavior in metallic glasses, Intermetallics 49 (2014) 52–56.
[35] X.N. Yang, C. Zhou, Q.J. Sun, L.N. Hu, J.C. Mauro, C.Z. Wang, Y.Z. Yue, Anomalous crystallization as a signature of the fragile-to-strong transition in metallic glass-forming liquids, J. Phys. Chem. B 118 (2014) 10258–10265.
[36] S. Yu, M. Kaviany, Electrical, thermal, and species transport properties of liquid eutectic Ga-In and Ga-In-Sn from first principles, J. Chem. Phys. 140 (2014) 064303.
[37] Y. Zhang, H.L. Zheng, Y. Liu, L. Shi, R.F. Xu, X.L. Tian, Cluster-assisted nucleation of silicon phase in hypoeutectic Al-Si alloy with further inoculation, Acta Mater. 70 (2014) 162–173.
[38] X.L. Zhao, X.F. Bian, J.Y. Qin, Y. Liu, Y.W. Bai, X.X. Li, L. Feng, K. Zhang, C.C. Yang, Unusual coordination structure in undercooled eutectic Ga-In alloy melt, Europhys. Lett. 107 (2014) 36004.
[39] Y.J. Lu, X.X. Zhang, M. Chen, J.Z. Jiang, Exploring the nature of the liquid-liquid transition in silicon: a non-activated transformation, Phys. Chem. Chem. Phys. 17 (2015) 27167–27175.
[40] J. Mosses, C.D. Syme, K. Wynne, Order parameter of the liquid-liquid transition in a molecular liquid, J. Phys. Chem. Lett. 6 (2015) 38–43.
[41] K. Murata, H. Tanaka, Microscopic identification of the order parameter governing liquid-liquid transition in a molecular liquid, Proc. Natl. Acad. Sci. 112 (2015) 5956–5961.
[42] F. Pacaud, M. Micoulaut, Thermodynamic precursors, liquid-liquid transitions, dynamic and topological anomalies in densified liquid germania, J. Chem. Phys. 143 (2015) 064502.
[43] R.Z. Li, J. Chen, X.Z. Li, E. Wang, L.M. Xu, Supercritical phenomenon of hydrogen beyond the liquid-liquid phase transition, New J. Phys. 17 (2015) 063023.
[44] F. Smallenburg, F. Sciortino, Tuning the liquid-liquid transition by modulating the Hydrogen-bond angular flexibility in a model for water, Phys. Rev. Lett. 115 (2015) 015701.
[45] W.L. Wang, Y.H. Wu, L.H. Li, W. Zhai, X.M. Zhang, B. Wei, Liquid-liquid phase separation of freely falling undercooled ternary Fe-Cu-Sn alloy, Sci. Rep. 5 (2015) 16335.
[46] L.H. Xiong, K. Chen, F.S. Ke, H.B. Lou, G.Q. Yue, B. Shen, F. Dong, S.Y. Wang, L.Y. Chen, C.Z. Wang, K.M. Ho, X.D. Wang, L.H. Lai, H.L. Xie, T.Q. Xiao, J.Z. Jiang, Structural and dynamical properties of liquid $Ag_{74}Ge_{26}$ alloy studied by experiments and ab initio molecular dynamics simulation, Acta Mater. 92 (2015) 109–116.
[47] W. Xu, M.T. Sandor, Y. Yu, H.B. Ke, H.P. Zhang, M.Z. Li, W.H. Wang, L. Liu, Y. Wu, Evidence of liquid-liquid transition in glass-forming $La_{50}Al_{35}Ni_{15}$ melt above liquidus temperature, Nat. Commun. 6 (2015) 7696.
[48] S.L. Zhang, L.M. Wang, X.Y. Zhang, L. Qi, S.H. Zhang, M.Z. Ma, R.P. Liu, Polymorphism in glassy silicon: inherited from liquid-liquid phase transition in supercooled liquid, Sci. Rep. 5 (2015) 8590.

[49] G. Zhao, Y.J. Yu, X.M. Tan, Nature of the first-order liquid-liquid phase transition in supercooled silicon, J. Chem. Phys. 143 (2015) 054508.
[50] K. Ito, C.T. Moynihan, C.A. Angell, Thermodynamic determination of fragility in liquids and a fragile-to-strong liquid transition in water, Nature 398 (1999) 492–495.
[51] T.T. Debela, X.D. Wang, Q.P. Cao, D.X. Zhang, J.Z. Jiang, The crystallization process of liquid vanadium studied by ab initio molecular dynamics, J. Phys. Condens. Matter 26 (2014) 155101.
[52] P. Ascarelli, Atomic radial distributions and ion-ion potential in liquid gallium, Phys. Rev. 143 (1966) 36.
[53] A.H. Narten, Liquid gallium: comparison of X-ray and neutron-diffraction data, J. Chem. Phys. 56 (1972) 1185.
[54] Y. Waseda, K. Suzuki, Structure factor and atomic distribution in liquid metals by X-ray diffraction, Phys. Status Solidi B 49 (1972) 339–347.
[55] S.E. Rodriguez, C. Pings, X-ray diffraction studies of stable and supercooled liquid gallium, J. Chem. Phys. 42 (1965) 2435.
[56] K.S. Vahvaselkä, Temperature dependence of the liquid structure of Ga, Phys. Scr. 22 (1980) 647.
[57] X. Gong, G.L. Chiarotti, M. Parrinello, E. Tosatti, Coexistence of monatomic and diatomic molecular fluid character in liquid gallium, Europhys. Lett. 21 (1993) 469.
[58] K.H. Tsai, T.M. Wu, S.F. Tsay, Revisiting anomalous structures in liquid Ga, J. Chem. Phys. 132 (2010) 034502.
[59] A.S. Basin, A.N. Solov'ev, Investigation of the density of liquid lead, cesium, and gallium by the gamma-method, J. Appl. Mech. Tech. Phys. 8 (1967) 57–59.
[60] H.V. Tippelskirch, Viscosities of cesium vapor to 1620 K and of liquid gallium to 1800 K, Ber. Bunsenges. Phys. Chem. 7 (1976) 726–729.
[61] G. Ginter, J.G. Gasser, R. Kleim, The electrical resistivity of liquid bismuth, gallium and bismuth-gallium alloys, Philos. Mag. B 54 (1986) 543–552.
[62] J. Vinckel, J. Hugel, J.G. Gasser, Electrical resistivity and absolute thermoelectric power of liquid silver-gallium alloys, Philos. Mag. B 73 (1996) 231–244.
[63] A.P. Hammersley, S.O. Svensson, M. Hanfland, A.N. Fitch, D. Hausermann, Two-dimensional detector software: from real detector to idealised image or two-theta scan, High Press. Res. 14 (1996) 235–248.
[64] X.Y. Qiu, J.W. Thompson, S.J.L. Billinge, PDFgetX2: a GUI-driven program to obtain the pair distribution function from X-ray powder diffraction data, J. Appl. Crystallogr. 37 (2004) 678.
[65] M.J. Assael, I.J. Armyra, J. Brillo, S.V. Stankus, J. Wu, W.A. Wakeham, Reference data for the density and viscosity of liquid cadmium, cobalt, gallium, indium, mercury, silicon, thallium and zinc, J. Phys. Chem. Ref. Data 41 (2012) 033101.
[66] J. Brillo, A. Bytchkov, I. Egry, L. Hennet, G. Mathiak, I. Pozdnyakova, D.L. Price, D. Thiaudiere, D. Zanghi, Local structure in liquid binary Al-Cu and Al-Ni alloys, J. Non Cryst. Sol. 352 (2006) 4008–4012.
[67] S.Y. Wang, M.J. Kramer, M. Xu, S. Wu, S.G. Hao, D.J. Sordelet, K.M. Ho, C.Z. Wang, Experimental and *ab initio* molecular dynamics simulation studies of liquid $Al_{60}Cu_{40}$ alloy, Phys. Rev. B 79 (2009) 144205.
[68] H.B. Lou, L.H. Xiong, A.S. Ahmad, A.G. Li, K. Yang, K. Glazyrin, H.P. Liermann, H. Franz, X.D. Wang, Q.P. Cao, D.X. Zhang, J.Z. Jiang, Atomic structure of $Pd_{81}Si_{19}$ glassy alloy under high pressure, Acta Mater. 81 (2014) 420–427.
[69] G. Kresse, J. Furthmüller, Efficiency of ab-initio total energy calculations for metals and semiconductors using a plane-wave basis set, Comp. Mater. Sci. 6 (1996) 15–50.
[70] G. Kresse, J. Furthmüller, Efficient iterative schemes for ab initio total-energy calculations using a plane-wave basis set, Phys. Rev. B 54 (1996) 11169.
[71] S. Nosé, A unified formulation of the constant temperature molecular dynamics methods, J. Chem. Phys. 81 (1984) 511.
[72] W.G. Hoover, Canonical dynamics: equilibrium phase-space distributions, Phys. Rev. A 31 (1985) 1695.
[73] P.E. Blöchl, Projector augmented-wave method, Phys. Rev. B 50 (1994) 17953.
[74] J.P. Perdew, K. Burke, M. Ernzerhof, Generalized gradient approximation made simple, Phys. Rev. Lett. 77 (1996) 3865.
[75] D.V. Louzguine-Luzgin, R. Belosludov, A.R. Yavari, K. Georgarakis, G. Vaughan, Y. Kawazoe, T. Egami, A. Inoue, Structural basis for supercooled liquid fragility established by synchrotron-radiation method and computer simulation, J. Appl. Phys. 110 (2011) 043519.
[76] K. Georgarakis, D.V. Louzguine-Luzgin, J. Antonowicz, G. Vaughan, A.R. Yavari, T. Egami, A. Inoue, Variations in atomic structural features of a supercooled Pd-Ni-Cu-P glass forming liquid during in situ vitrification, Acta Mater. 59 (2011) 708–716.
[77] N.A. Mauro, M. Blodgett, M.L. Johnson, A.J. Vogt, K.F. Kelton, A structural signature of liquid fragility, Nat. Commun. 5 (2011) 4616.
[78] K. Georgarakis, L. Hennet, G.A. Evangelakis, J. Antonowicz, G.B. Bokas, V. Hokimaki, A. Bytchkov, M.W. Chen, A.R. Yavari, Probing the structure of a liquid metal during vitrification, Acta Mater. 87 (2015) 174–186.
[79] P.J. Steinhardt, D.R. Nelson, M. Ronchetti, Bond-orientational order in liquids and glasses, Phys. Rev. B 28 (1983) 784.
[80] W. Mickel, S.C. Kapfer, G.E. Schroder-Turk, K. Mecke, Shortcomings of the bond orientational order parameters for the analysis of disordered particulate matter, J. Chem. Phys. 138 (2013) 044501.
[81] H. Zhang, C. Zhong, J.F. Douglas, X.D. Wang, Q.P. Cao, D.X. Zhang, J.Z. Jiang, Role of string-like collective atomic motion on diffusion and structural relation in glass forming Cu-Zr alloys, J. Chem. Phys. 142 (2015) 164506.
[82] X.W. Fang, C.Z. Wang, Y.X. Yao, Z.J. Ding, K.M. Ho, Atomistic cluster alignment method for local order mining in liquids and glasses, Phys. Rev. B 82 (2010) 184204.
[83] S. Wu, M.J. Kramer, X.W. Fang, S.Y. Wang, C.Z. Wang, K.M. Ho, Z.J. Ding, L.Y. Chen, Structural and dynamical properties of liquid $Cu_{80}Si_{20}$ alloy studied experimentally and by *ab initio* molecular dynamics simulations, Phys. Rev. B 84 (2011) 134208.
[84] X.W. Fang, C.Z. Wang, S.G. Hao, M.J. Kramer, Y.X. Yao, M.I. Mendelev, Z.J. Ding, R.E. Napolitano, K.M. Ho, Spatially resolved distribution function and the medium-range order in metallic liquid and glass, Sci. Rep. 1 (2011) 194.
[85] F.S. Ke, G.Q. Yue, B. Shen, F. Dong, S.Y. Wang, Y.X. Zheng, L.Y. Chen, C.Z. Wang, K.M. Ho, Bergman-type medium-range order in rapidly quenched Ag0.74Ge0.26 eutectic alloy studied by ab initio molecular dynamics simulation, Acta Mater. 80 (2014) 498–504.
[86] H. Tanaka, General view of a liquid-liquid phase transition, Phys. Rev. E 62 (2000) 6968.
[87] G.D. Fontana, L. Battezzati, Thermodynamic and dynamic fragility in metallic glass-formers, Acta Mater. 61 (2013) 2260–2267.
[88] M.E. Blodgett, T. Egami, Z. Nussinov, K.F. Kelton, Proposal for universality in the viscosity of metallic liquids, Sci. Rep. 5 (2015) 13837.